Available online at www.sciencedirect.com
SCIENCE DIRECT®
Sensors and Actuators A xxx (2004) xxx–xxx
SENSORS AND ACTUATORS A PHYSICAL
www.elsevier.com/locate/sna

High-power optical microswitch based on direct fiber actuation

Kevin R. Cochran[a,b,*], Lawrence Fan[b], Don L. DeVoe[a]

[a] *Department of Mechanical Engineering, University of Maryland, College Park, MD 20742, USA*
[b] *Indian Head Division, Naval Surface Warfare Center, Bldg. 302, 101 Strauss Avenue, Indian Head, MD 0640, USA*

Received 12 May 2004; received in revised form 14 September 2004; accepted 30 October 2004

Abstract

An optical microswitch is presented for high-power switching applications. The device, capable of switching several watts of optical power, employs large-core multimode fibers to switch output from a laser diode operating at a wavelength of 810 nm. Switching is achieved through the direct deflection of an on-chip fiber using a high force electrothermal actuator. Optical losses in the system are identified, and optical efficiency is predicted and verified with experimental measurements. The switch demonstrated in this work requires an electrical current of 120 mA and has an electrical power consumption of 5280 mW. The optical efficiency is found to be on the order of 88% (0.55–0.60 dB loss) with a maximum power transfer of 1690 mW from a 1930 mW input. Switching time is 40 ms with channel isolation between the on and off states of 55 dB.

Keywords: MOEMS; DRIE; Thermal actuator; High-power; Optical switch

1. Introduction

An optical microswitch designed for high-power switching applications has been developed. The switch is based on the direct actuation of optical fibers using electrothermal microactuators fabricated by deep reactive-ion etching (DRIE) of silicon-on-insulator (SOI) wafers. In this "bending fiber" design, a pair of input and output optical fibers are actuated from an out-of-line to in-line position, so that optical power transfer can take place. The device is intended for applications requiring the transfer of high-power optical energy, on the order of several watts, and hence avoids the use of reflective or blocking elements to alter the optical path, which can be susceptible to damage from high-power optical energy.

Macro switches based on directly actuating optical fibers have been available for some time [1–4]. These macro switches most often hold the fibers in an alignment sleeve and use magnetic actuation to move the fibers in and out of alignment. Macro-scale bending fiber switches that use some assembled micromachined parts have also appeared previously [5–8]. These switches use micromachined parts such as v-groove fiber holders and positioning stages in conjunction with macro parts, such as electromagnetic actuators, to create a complete switch.

Most of the fully micromachined optical switches that have appeared in recent years are based on actuating a micromachined reflector or blocking element in and out of the optical path between input and output fibers. However, fully micromachined bending fiber type switches have also been demonstrated [9–12] using actuators, such as electrostatic [9] or electrothermal [10–12] designs that are capable of producing the high forces and displacements required to bend optical fibers. Moving waveguide optical switches have also been demonstrated based on micromachined integrated waveguides instead of attached optical fibers [13–16].

There are several differences between the switch discussed in this work and previously demonstrated bending fiber type switches. Fabrication is a simple process consisting of a metal deposition followed by a single front side etch and subsequent release, compared with previously reported designs which require an additional backside wafer etch [10,11]

* Corresponding author. Tel.: +1 301 744 1163; fax: +1 301 744 6406.
E-mail address: cochrankr@ih.navy.mil (K.R. Cochran).

0924-4247/$ – see front matter © 2004 Elsevier B.V. All rights reserved.
doi:10.1016/j.sna.2004.10.037

or attachment of a top wafer [9–11] for device operation. Additionally, the actuator design has been optimized using an analytic model. Actuator size has been minimized, with a length scale on the order of 5 mm compared with between 7.4 mm [12] and 20 mm [9–11] in previous work. Switching speed has also been reduced to 40 ms, compared with between 100 ms [10] and several hundred milliseconds [11,12]. Finally, an important and unique feature of the present work is the demonstration of high-power optical switching through coupled multimode fibers with losses well below 1 dB.

Specifically, the device was designed for optical power transfer in a MEMS based safety and arming system (S&A) for underwater weapons applications [17,18], in which a 1×1 switch configuration is used to transfer optical power between input and output fibers in the on state, with no power transferred in the off state. A previous reflector-based optical microswitch designed for this application [18] exhibited an average optical efficiency of only 55% (2.6 dB loss) due to light scattering introduced by reflector surface roughness. The bending fiber switch design described in this work was motivated by the desire to improve the optical efficiency, while allowing for power transfer greater than 1 W. Note that while a 1×1 switch is investigated here to meet the needs of the S&A application, the switch design is readily scalable to a 1×2 configuration for other high-power switching applications.

In the bending fiber type optical microswitch, a v-beam electrothermal actuator is used to push opposing optical fibers in and out of direct alignment with each other. For the S&A application, the switch is configured so that the fibers are initially offset in the out-of-line (off) position and are then actuated to the in-line (on) position, but this configuration can easily be reversed. A schematic diagram of the switch concept is shown in Fig. 1, and the general switch layout is shown in Fig. 2. The optical fibers are placed in etched alignment channels on the chip surface for ease of assembly, with initial fiber axes offset by one fiber diameter to ensure minimal light transmission in the off state. The input channel is widened a certain distance, *C*, before the endface of the fiber to create a cantilevered fiber section. The thermal actuator is placed very near the cleaved fiber face to minimize the cantilevered fiber length, thereby improving the switch response time.

Fabrication is performed using a single DRIE etch to create both the fiber alignment channels and actuators. SOI substrates are utilized for controllable actuator thickness, while enabling actuators to be released with a timed HF etch. The Si device layer thickness used in this work is 125 μm, ensuring that fiber centerlines contact the sidewalls of the patterned features, and providing sufficient actuation force to satisfy switch requirements.

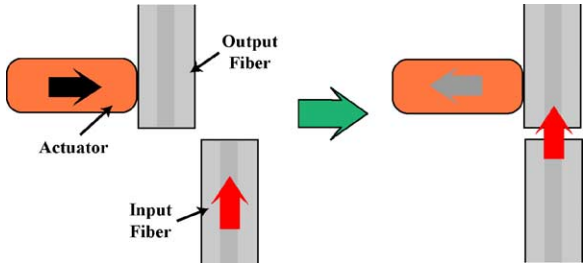

Fig. 1. Operation of the bending fiber type optical switch.

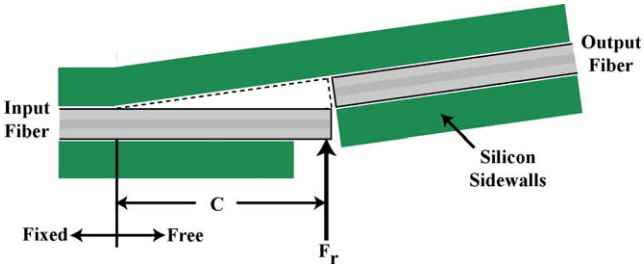

Fig. 2. Schematic layout of the bending fiber optical switch.

2. System optical analysis

Optical losses will be incurred in the moving-fiber type switch due to two primary mechanisms, namely Fresnel reflections at the fiber glass–air interfaces, and mechanical misalignments between the fibers. Fig. 3 shows the alignment of the input and output fibers. The optical power exiting the input fiber is designated P_{IN}, while the optical power exiting the output fiber is designated P_{OUT}. Although Fresnel reflection losses occur at the glass–air interfaces present at each end of both the input and output fibers, those at the input fiber are ignored because P_{IN} is directly measured. Misalignment losses (L_S) are incurred because the input and output fiber endfaces are separated by a gap, *s*. The system optical efficiency is taken as the ratio P_{OUT}/P_{IN} and can be found as

$$\frac{P_{OUT}}{P_{IN}} = (1 - R_F)^2(1 - L_S) \quad (1)$$

where R_F and L_S are given by the percentage of light lost due to Fresnel reflections and fiber misalignment, respectively. The Fresnel reflection loss represents the ratio of light reflected to total light incident on the glass–air interface and can be calculated using [19]

$$R_F = \left(\frac{n_c - n}{n_c + n}\right)^2 \quad (2)$$

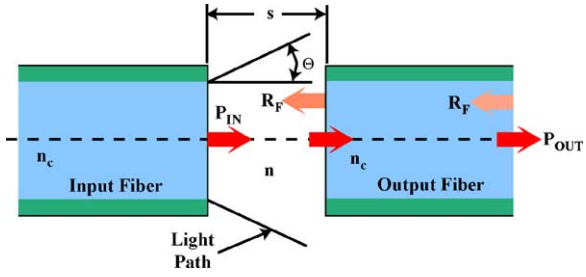

Fig. 3. Optical losses encountered in direct fiber to fiber transfer.

where n and n_c are the refractive indices of air ($n = 1$) and the output fiber core. For high-power optical switching, large-core multimode fibers with outside core/cladding diameters of 105/125 μm are used. The fibers have a numerical aperture (NA) of .22 and core refractive index of 1.453. Using these values, the loss at each glass–air interface due to Fresnel reflections is found to be 3.4%. The two reflections at the output fiber interfaces will therefore reduce the maximum achievable system optical efficiency to 93.3%.

Misalignment losses between optical fibers can result from axial offset, angular offset, and longitudinal separations [19]. In the present design, the input fiber is actuated against the silicon sidewall and the output fiber is held in a precise alignment channel (see Fig. 2) so that losses due axial and angular misalignments are assumed to be negligible. Therefore, any misalignment losses will be due solely to longitudinal fiber separation. The coupling efficiency (P_{OUT}/P_{IN}) for two fibers of equal core diameter, separated by a gap, s, can be calculated using a geometrical optics approach. From [20], the fiber coupling efficiency, η, is given by

$$\eta = \frac{4}{\pi(\mathrm{NA})^2}\int_0^w \left[\arccos\left(\frac{\zeta w}{2}\right) - \left(\frac{\zeta w}{2}\right)\sqrt{1-\left(\frac{\zeta w}{2}\right)^2}\right] \times \frac{w}{(1+w^2)^2}\,\mathrm{d}w \quad (3)$$

with w defined as

$$w = \min\left(\frac{\mathrm{NA}}{\sqrt{1-\mathrm{NA}^2}}, \frac{2}{\zeta}\right) \quad (4)$$

In Eqs. (3) and (4), $w = \tan\Theta$, and $\varsigma = s/a$, where Θ is the divergence half angle of the light exiting the input fiber and a is the fiber core radius. The NA of the fibers used (.22) corresponds to a divergence half angle of 12.7°. Note that $\eta = 1 - L_S$, as outlined in Eq. (1).

The switch is designed so that the minimum separation between input and output fibers is 10 μm when the fibers are butted against the silicon end stops, ensuring adequate clearance during switching. It is also necessary to back the actuated fiber away from the end stop slightly during assembly, to ensure that friction between fiber and end stop will not prevent smooth motion of the actuated fiber. Measured fiber separation is often increased to as much as 15 μm, resulting in a coupling efficiency ($1 - L_S$) of 97.3% using Eq. (3).

The overall system optical efficiency can now be predicted using Eq. (1). The predicted Fresnel reflection loss of 6.7% and separation loss of 2.7% results in a maximum achievable system efficiency of 90.8% (0.42 dB loss).

3. Actuator development

3.1. Force and displacement requirements

As stated earlier, in order to ensure that minimal optical power transfer takes place in the out-of-line position, the input and output fiber centerline axes are offset by one fiber diameter. This offset is 125 μm for the fibers in this study, so that the actuated fiber tip must be displaced 125 μm. With the actuator very near the end of the fiber, the required actuator displacement, u_r, is thus approximately the same as the fiber tip displacement. The end of the actuator is also offset from the edge of the fiber channel by 5 μm to ensure adequate clearance during assembly so that the final required actuator displacement is 130 μm.

A mechanical analysis of the fiber is necessary in order to determine the required actuator force output. The fiber is treated as a cantilevered beam with circular cross section as shown in Fig. 4. The required actuator force, F_r, can then be found from [21]

$$F_r = \frac{3u_r EI}{C^3} \quad (5)$$

where

$$I = \tfrac{1}{4}\pi r^4 \quad (6)$$

In Eqs. (5) and (6), C is the fiber cantilever length, r is the outside fiber cladding radius, I is the fiber moment of inertia, and E is the fiber elastic modulus. Silica fibers are used and E is taken as 71 GPa [22]. It is assumed that friction between the fiber and underlying silicon substrate will be negligible.

Fig. 5 shows the required actuator force versus fiber cantilever length (with $u_r = 130$ μm) calculated using Eq. (5). Actuators have been designed for cantilever lengths ranging from 2500 to 4000 μm, requiring corresponding actuator forces ranging from 20.9 to 5.1 mN.

3.2. Actuator design model

A v-beam electrothermal actuator design is chosen due to the high force and displacement required to move the optical fibers. A v-beam electrothermal actuator consists of a clamped beam with a slight offset in the middle. When electrical current is applied across the beam, Joule heating causes

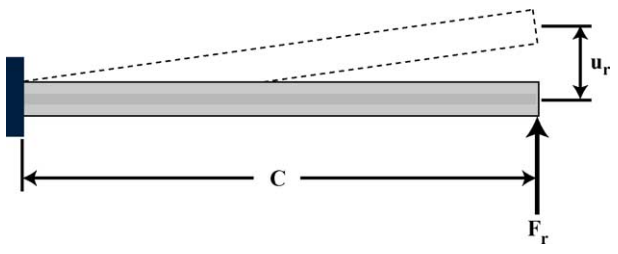

Fig. 4. Optical fiber cantilever model. F_r = actuator force and u_r = fiber tip displacement.

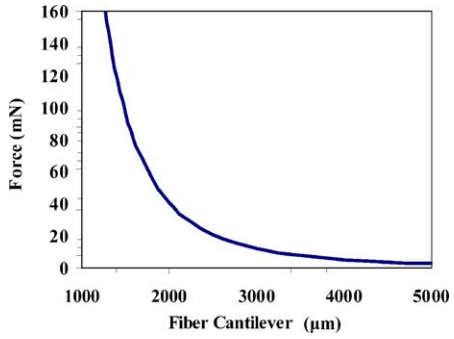

Fig. 5. Required actuator force vs. fiber cantilever length, with fiber tip displacement = 130 μm.

the beam to expand and deflect in the direction of the offset as depicted in Fig. 6. An actuator with a higher force output can be realized by placing several of the beams in parallel with shared anchors and a central yoke.

A model developed by Maloney et al. [23] has been used to design the v-beam electrothermal actuators, with the important points outlined in the following for clarity. The constants and variables used in the model are shown in Table 1. In this model, an electrothermal analysis is used to find the temperature distribution along the length of the actuator beam and the resulting thermal expansion in the material. This is done by solving the heat equation, with the appropriate boundary conditions, resulting from a 1D cross-sectional energy balance of the beam. The thermal conductivity, k_s, and thermal expansion coefficient (CTE), α, of the silicon are temperature dependent so that the expressions that describe the beam temperature and thermal expansion become non-linear. The thermal conductivity decreases with increasing temperature while the CTE increases with temperature. A computer program, written in MATLAB, is used to solve the non-linear temperature and thermal expansion equations. The beam is divided into elements and iterations are performed until a specified degree of convergence is reached.

A thermomechanical analysis employing the method of virtual work and linear beam theory is then used to find the net maximum midpoint displacement and maximum force resulting from the thermal expansion in the beam. From this

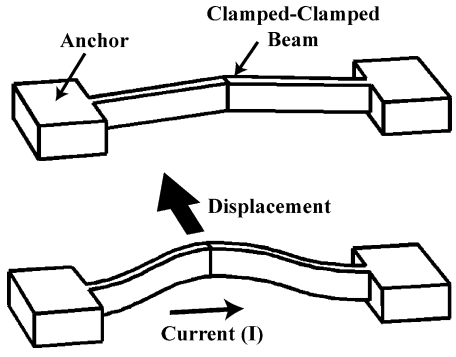

Fig. 6. The v-beam thermal actuator design and operation.

Table 1
Constants and variables used in the v-beam thermal actuator design model

	Parameter	Value
g	Gap between beams and substrate	2 μm
h	Height of beams	125 μm
L	Length of beams	–
d	Central offset of beam	–
w	Width of beam	–
J	Current density	–
k_a	Thermal conductivity, air	0.026 W/m K
k_s	Thermal conductivity, silicon	42–148 W/m K
α	Thermal expansion coefficient, silicon	$(2.6–4.1) \times 10^{-6}$ K^{-1}
c	Specific heat, silicon	700 J/kg K
E	Elastic modulus, silicon	166 GPa
ρ	Resistivity, silicon	0.016 Ω cm

model, the maximum beam deflection, u_t, and maximum force output, F_t, are found to be approximately equal to the following

$$\frac{u_t}{P} = \frac{\alpha L d}{4whk_s m^2(d^2 + w^2)} \left[1 - \frac{2\tanh(mL/2)}{mL}\right] \tag{7}$$

$$\frac{F_t}{P} = \frac{4\alpha E d}{k_s m^2 L^2} \left[1 - \frac{2\tanh(mL/2)}{mL}\right] \tag{8}$$

with

$$m^2 = \frac{Sk_a}{k_s gh} \tag{9}$$

The equations are stated on a per unit electrical power basis, with the power, P, equal to

$$P = whLJ^2\rho \tag{10}$$

The shape factor, S, represents the ratio of heat loss from the sides and bottom of the beam to the heat loss from the bottom of the beam only. From finite element analysis of the 125 μm tall actuators in this study, S has been found to be equal to 4.56 [24]. Eqs. (7) and (8) predict infinite deflection and force as the current is increased but the actual deflection and force are limited by the intrinsic point temperature of the silicon. This temperature is dependent upon the level of doping present in the silicon and is estimated to be 800 K for the wafers used in this study [25].

The v-beam electrothermal actuators exhibit a linear relationship between deflection and force, with maximum force occurring at zero displacement and the minimum force occurring at maximum displacement. Due to this linear relationship, the following equation can be written

$$\frac{u_t - u_r}{u_t} = \frac{F_r}{nF_t} \tag{11}$$

In Eq. (11), the maximum total actuator force is equal to the maximum force produced by a single beam, F_t, multiplied by the number of beams, n. Since the available force is proportional to the difference between u_t and u_r, u_t needs to be made much larger than u_r in order that the force available at u_r is at least equal to F_r.

Table 2
Effects of thermal actuator design variables on actuator performance parameters

Parameter	Effect on actuator performance		
	F_t/P	u_t/P	F_{cr}
Increased beam length (L)	–	+	–
Increased beam width (w)	N/A	–	+
Increased beam offset (d)	+	–	+
Increased # beams (n)	+	N/A	N/A[a]

[a] Effect on critical load per beam.

As a final design criteria, actuator beam buckling under load during operation is considered. If it is assumed that the midpoint of the beam is fixed, the critical buckling load, F_{cr}, can be approximated by [26]

$$F_{cr} = \frac{16\pi^2 whdE(d^2 + w^2)}{3L^3} \quad (12)$$

For the actuator designs, the critical buckling load is kept above (1.5–2 times) the maximum force, F_t, that a single actuator beam is capable of producing.

It is useful to develop a design strategy in order to efficiently design actuators based on the beam geometry design variables (L, w, d, n). The variables can then be optimized based on specific design criteria such as minimizing power consumption. By using Eqs. (7), (8) and (12), the effects of changing the beam geometry design variables versus the displacement and force output per unit power as well as the critical buckling load are found and are summarized in Table 2. In this table, + and – indicate either an increase or a decrease in the performance parameter and N/A indicates that changing the design variable has no effect on that particular parameter.

A few important points should be noted. The beam width should be made as small as the buckling criteria will allow in order to increase u_t without effecting F_t. There is a tradeoff between increasing the beam length in order to increase u_t and decreasing F_t and F_{cr}. Increasing the beam offset has the opposite effect of increasing the beam length in that F_t and F_{cr} will both increase but u_t will decrease.

4. Experimental results and discussion

4.1. Fabrication

Device fabrication was performed at MEMSCAP (formerly JDS Uniphase, MEMS Business Unit) in Research Triangle Park, NC. Processing consisted of a Cr/Au (200/5000 Å thickness) evaporation and liftoff step to create bond pads on a 4 in. SOI wafer with a 125 μm thick device layer. This was followed by a DRIE etch to define fiber alignment channels and actuators. Next, a concentrated HF dip removes the 2 μm buried oxide layer for actuator release. Next, a CO_2 super critical drying step is performed to prevent stiction of released devices. Fibers were inserted in the alignment channels and the actuated fiber manually adjusted to position the endface as close to the mechanical stops as possible without actually touching. The fibers were prepared with a straight cleave and left unpolished, and secured to the channels by epoxy. SEM micrographs of fabricated devices with attached optical fibers are shown in Fig. 7a and b.

4.2. Actuator measurements

The v-beam electrothermal actuators have been characterized to ensure that their behavior is accurately predicted by the design model. This is done by measuring actuator displacement versus input drive current. Measurements are made with and without optical fibers in place in order to determine the maximum free displacement of each actuator. Actuator displacement is measured by observing a scale etched into the silicon substrate next to the actuator fiber pusher arm, with a measurement resolution of 2 μm.

A plot of measured actuator deflection versus applied current for one of the actuator designs is shown in Fig. 8. The beam geometry and fiber cantilever length are outlined on the plot. This particular actuator design uses two long and thin beams to achieve a reasonably high u_t/P ratio. The beam offset is adjusted so that the required force and buckling criteria are achieved. While a range of actuator designs were fabricated, the results shown here are based on an actuator

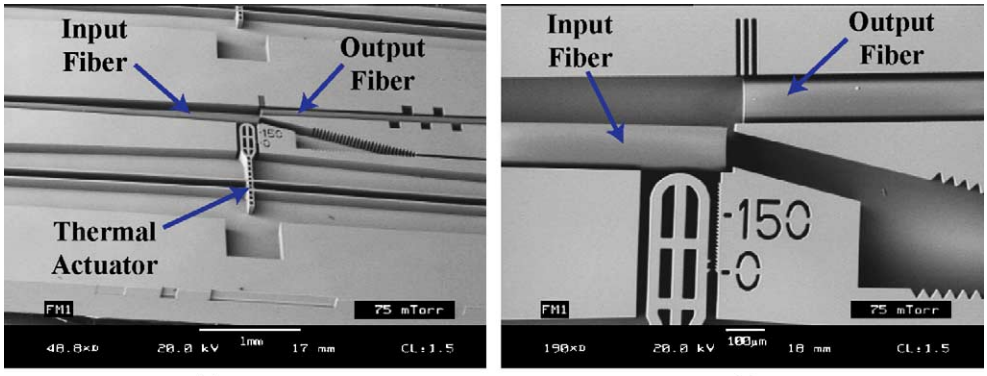

Fig. 7. SEM micrographs showing (a) bending fiber type optical microswitch and (b) fiber and actuator alignment.

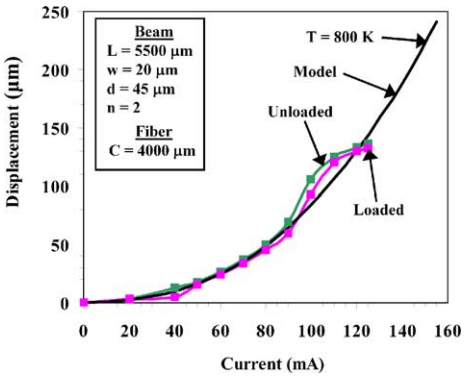

Fig. 8. The v-beam thermal actuator displacement vs. drive current.

geometry of $L = 5500\ \mu m$, $w = 20\ \mu m$, $d = 45\ \mu m$, $n = 2$, and a fiber cantilever length of $C = 4000\ \mu m$. For this actuator design, the fiber is observed to hit the silicon channel sidewall (130 μm actuator displacement) at a current of 120 mA and voltage of 44 V for a total required power of 5280 mW. The voltage requirements are approximately 50% higher than expected due to high bond pad contact resistance. Maximum unloaded actuator throw is 136 μm at a current of 125 mA.

As can be seen, the actuator behavior follows the model with good agreement. This has also been demonstrated with similar actuator designs in previous work [23,24,26]. However, the deflection rolls off before the estimated 800 K intrinsic point of the silicon. This effect was observed for all actuator designs tested. The behavior is believed to be due, in part, to a lower intrinsic point than expected in the silicon. Also, it has been observed that, in general, a multiple beam actuator will have a reduced maximum deflection over a single beam actuator with the same beam dimensions. This is believed to be due to a "weakest link" effect. Due to mask tolerances and beam undercutting, each beam in a multi-beam actuator will have a slightly different cross-sectional area. The beams will heat differently and thus not produce the same thermal strain. The end result is that the cooler beams become a burden to the hotter beams. This effect is not accounted for in the model. It should also be noted that as the current is increased and the actuator beam temperature increases beyond the intrinsic point, the silicon begins to glow. The operational range of the actuator should be kept below this point to avoid possible plastic deformation under load or melting of the actuator beams.

4.3. Switching measurements

Complete switch devices have also been characterized in order to determine switching speed and optical efficiency at high-power levels. Optical power is supplied from a 2000 mW, 810 nm laser diode (B&W Tek BWK-810-2W-pig) pigtailed with a 105 μm core multimode fiber. The laser diode is driven with a laser diode driver (Newport 5060). This source was chosen in order to evaluate the high-power optical performance of the switch. Output optical power is monitored with a silicon detector (Newport 818-SL) and power meter (Newport 1815-C). Electrical power is supplied by a power supply and function generator. Actuator power input and detector output are also monitored with an oscilloscope.

The optical efficiency for the switch has been found to range from 87 to 88% (0.55–0.60 dB insertion loss) for all devices tested. Maximum power transferred from a 1930 mW (measured) optical input was 1690 mW. Optical efficiency is slightly less than that predicted by the optical efficiency model (0.42 dB loss), likely due to imperfections such as scratches on the endfaces of the optical fibers that scatter light. Optical efficiency can potentially be improved by using polished, rather than as-cleaved fibers. An anti-reflection coating on the fiber endfaces will also greatly decrease the Fresnel reflection losses and improve the theoretical optical efficiency of the switch to approximately 95% (0.22 dB insertion loss). It should also be noted that no damage to the optical fibers due to the high-power optical energy transfer between their endfaces was observed during any tests.

Optical efficiency measurements were also performed using single mode fibers. In this case, switch losses were found to range from 1.5 to 2.5 dB, compared with theoretical losses of 1.7 dB for a single mode fiber configuration [27].

A plot of photodetector output versus actuator input for one of the switches is shown in Fig. 9. The switch uses the thermal actuator outlined in the previous section. Switching time from the out-of-line to in-line position took 40 ms, while a return to the out-of-line position took 11 ms. Channel isolation was observed to be very good at 55 dB.

Measurements were also performed to determine the maximum switching frequency of the bending fiber switch. The actuators were driven with a 50% duty cycle, square wave input. The maximum switching frequency was found to be 20 Hz. Above this point, the optical power would no longer reach the maximum low-frequency value at each switching cycle.

While the S&A application that the bending fiber switch has been designed for requires the actuator to operate only once for a relatively short period of time, other applications may require the actuator to operate for a sustained period at full deflection, resulting in excessive chip heating. Successful

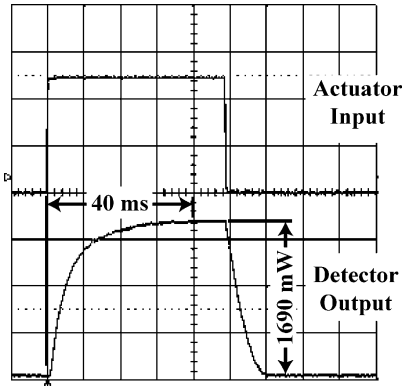

Fig. 9. Actuator input vs. detector output, showing dynamic switching characteristics of the optical switch.

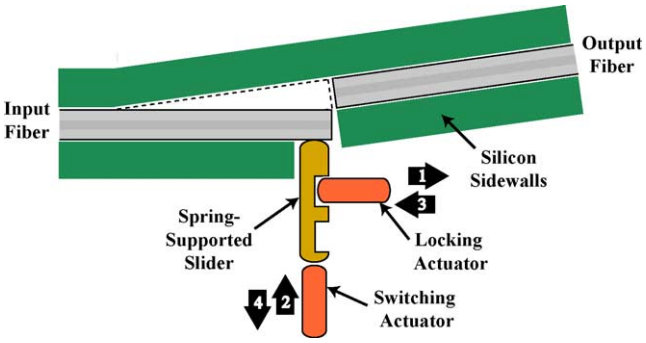

Fig. 10. Schematic layout of a bi-stable bending fiber type optical switch. Numbered arrows indicate operational sequence of the actuators and slider.

operation will depend on the ability to provide sufficient heat sinking, assuming that the required electrical power is available. Although long-term continuous operation of the optical switch has not been explored here, similar v-beam thermal actuator designs have been shown to be reliable for at least 60×10^6 cycles at an operational frequency of 50 Hz [26].

Furthermore, the switch design is amenable to operation in a bistable mode with the addition of a secondary locking actuator and spring-supported, movable slider. A schematic layout of this concept is shown in Fig. 10. In this design, the locking actuator is first retracted from a detent in the slider and the switching actuator pushes the slider and the output fiber to the in-line position. The two actuators are then returned to an un-powered state with the locking actuator mating to a second detent in the slider, thus holding the output fiber in the in-line state. Switches based on this bistable concept have recently been fabricated and are undergoing evaluation.

5. Conclusion

The switching of high levels of optical power in a micromachined device has been successfully demonstrated by taking advantage of direct electrothermal actuation of cantilevered large-core multimode fibers. Actuator displacement versus drive current was found to be in good agreement with model predictions. The switch was demonstrated using an 810 nm, 2000 mW LD with 105 μm core diameter multimode input and output fibers. Optical transfer efficiency of 87–88% (.55–.60 dB loss) was observed with a maximum power transfer of 1690 mW. The power handling of the switch is currently limited only by the availability of suitable high-power laser diode sources, and significantly higher power transfer may be feasible as higher power sources become available.

Acknowledgments

The authors would like to thank DARPA and the Office of Naval Research for the funding and continued support of this research. The authors also would like to thank Dr. Brandon Choi for the SEM micrographs.

References

[1] A. Gurbaxani, Fully-reversible 'moving fiber' switch permits enhanced applications, in: Proceedings of the SPIE on Components for Fiber Optic Applications II, vol. 839, 1987, pp. 67–72.
[2] H. Yamamoto, H. Ogiwara, Moving optical-fiber switch experiment, Appl. Opt. 17 (1978) 3675–3678.
[3] S. Aoki, T.P. Tanaka, M. Maeda, H. Takashima, Paired optical-fiber switch for optical data-bus systems, Opt. Lett. 4 (1979) 346–347.
[4] P.G. Hale, R. Kompener, Mechanical optical-fibre switch, Electron. Lett. 12 (1976) 388.
[5] J.H.C. van Zantvoort, F.M. Huijskens, C.G.P. Herben, H. de Waardt, Fiber-array pigtailing and packaging of an InP-based optical cross-connect chip, IEEE J. Sel. Top. Quant. Electron. 5 (1999) 1255–1259.
[6] S. Nagaoka, Compact latching-type single-mode-fiber switches fabricated by a fiber-micromachining technique and their practical applications, IEEE J. Sel. Top. Quant. Electron. 5 (1999) 36–45.
[7] C. Gonzalez, S.D. Collins, Magnetically actuated fiber-optic switch with micromachined positioning stages, Opt. Lett. 22 (1997) 709–711.
[8] R.A. Norwood, J. Holman, L.W. Shacklette, S. Emo, N. Tabatabaie, H. Guckel, Fast, low insertion loss optical switch using lithographically defined electromagnetic microactuators and polymeric passive alignment structures, Appl. Phys. Lett. 73 (1998) 3187–3189.
[9] M. Hoffmann, D. Nusse, E. Voges, Electrostatic parallel-plate actuators with large deflections for use in optical moving-fibre switches, J. Micromech. Microeng. 11 (2001) 323–328.
[10] F. Pieri, M. Piotto, A micromachined bistable 1×2 switch for optical fibers, Microelectron. Eng. 53 (2000) 561–564.
[11] P. Kopka, M. Hoffmann, E. Voges, Coupled U-shaped cantilever actuators for 1×4 and 2×2 fiber switches, J. Micromech. Microeng. 10 (2000) 260–264.
[12] L.A. Field, D.L. Burriesci, P.R. Robrish, R.C. Ruby, Micromachined 1×2 optical-fiber switch, Sens. Actuators A: Phys. 53 (1996) 311–315.
[13] E. Ollier, P. Mottier, Integrated electrostatic microswitch for optical fibre networks driven by low voltage, Electron. Lett. 32 (1996) 2007–2008.
[14] T. Bakke, C.P. Tigges, C.T. Sullivan, Silicon-on-insulator micromechanical optical switch with post processed polymeric waveguides, in: Proceedings of the SPIE on MOEMS Miniaturized Systems II, vol. 4561, 2001, pp. 85–92.
[15] G.J. Veldhuis, T. Nauta, C. Gui, J.W. Berenschot, P.V. Lambeck, Electrostatically actuated mechanooptical waveguide on–off switch showing high extinction at a low actuation-voltage, IEEE J. Sel. Top. Quant. Electron. 5 (1999) 60–65.
[16] F. Chollet, M. de Labachelerie, H. Fujita, Compact evanescent optical switch and attenuator with electromechanical actuation, IEEE J. Sel. Top. Quant. Electron. 5 (1999) 52–59.
[17] L. Fan, H. Last, R. Wood, B. Dudley, C.K. Malek, Z. Ling, SLIGA based underwater weapon safety and arming system, Microsyst. Technol. 4 (1998) 168–171.
[18] K.R. Cochran, D.L. DeVoe, L. Fan, Moving reflector type micro optical switch for high-power transfer in a MEMS-based safety and arming system, J. Micromech. Microeng. 14 (2004) 138–146.
[19] G. Keiser, Optical Fiber Communications, McGraw-Hill, Boston, 2000.
[20] W. van Etten, W. Lambo, P. Simons, Loss in multimode fiber connections with a gap, Appl. Opt. 24 (1985) 970–976.
[21] F.P. Beer, E.R. Johnston Jr., Mechanics of Materials, McGraw-Hill, New York, 1992.

[22] Fiberguide Industries, Mechanical Data of Fused Silica, Manufacturer Data Sheet.
[23] J.M. Maloney, D.S. Schreiber, D.L. DeVoe, Large-force electrothermal linear micromotors, J. Micromech. Microeng. 14 (2004) 226–234.
[24] K.R. Cochran, Development of a micro optical switch fabricated by deep reactive ion etching (DRIE) for high-power transfer applications, MS Thesis, University of Maryland, 2003.
[25] G.L. Pearson, J. Bardeen, Electrical properties of pure silicon and silicon alloys containing boron and phosphorus, Phys. Rev. 75 (1949) 865–883.
[26] J. Maloney, Fabrication and thermal actuation of three dimensional micro electro mechanical systems, MS Thesis, University of Maryland, 2001.
[27] S. Nemota, T. Makimoto, Analysis of splice loss in single-mode fibers using a gaussian field approximation, Opt. Quant. Electron. 11 (1979) 447–457.

Biographies

Kevin R. Cochran received the BS and MS degrees in Mechanical Engineering from the University of Maryland, College Park in 1998 and 2003, respectively. He is currently employed with the Indian Head Division, Naval Surface Warfare Center in Indian Head, MD. Since 1998, he has performed research and development in the areas of microelectromechanical systems (MEMS) and their application to Fuze/Safety and Arming systems. His work is currently focused on optical MEMS design and MEMS packaging. He has co-authored several papers and has two pending patents in the areas of MEMS design and packaging.

Lawrence Fan is a senior mechanical engineer in the Warheads Technology and Development Department at Indian Head Division, NAVSEA. Since 1990, he has been a technical specialist and manager of fuzing and safe-arm device development. His current position, which he has held since 2000, is the program manager for MEMS Fuze/Safe and Arm (F/S&A) in the 6.75 in. diameter canistered countermeasure anti-torpedo. He previously served a fuze designer on the development teams for the APOBS fuze, Navy gun-fired projectiles, including MK 419 multi-function fuze, MK 22 Exploder, ENATD fuze and the MEMS technology for fuze/S&A. He is recognized in the international and DoD community for his work in MEMS and Fuzing/S&A and has regularly published in MEMS and DoD forums, including HARMST, DARPA MEMS MTO, and NDIA. He is also a co-inventor on three MEMS and Fuze/S&A related patents and has another patent pending.

Don L. De Voe is an associate professor of mechanical engineering at the University of Maryland, College Park, where he is an affiliate faculty with the Bioengineering Graduate Program. He received a PhD degree in mechanical engineering from the University of California, Berkeley, in 1997. He is a recipient of the Presidential Early Career Award for Scientists and Engineers from the National Science Foundation, with research interests including microfluidic systems for genomic and proteomic analysis, and novel microfabrication methods including nano-scale polymer replication techniques.